Rational catalyst and electrolyte design for CO_2 electroreduction towards multicarbon products

Dunfeng Gao [ID], Rosa M. Arán-Ais, Hyo Sang Jeon [ID] and Beatriz Roldan Cuenya*

The CO_2 electroreduction reaction (CO_2RR) to fuels and feedstocks is an attractive route to close the anthropogenic carbon cycle and store renewable energy. The generation of more reduced chemicals, especially multicarbon oxygenate and hydrocarbon products (C_{2+}) with higher energy densities, is highly desirable for industrial applications. However, selective conversion of CO_2 to C_{2+} suffers from a high overpotential, a low reaction rate and low selectivity, and the process is extremely sensitive to the catalyst structure and electrolyte. Here we discuss strategies to achieve high C_{2+} selectivity through rational design of the catalyst and electrolyte. Current state-of-the-art catalysts, including Cu and Cu–bimetallic catalysts, as well as some alternative materials, are considered. The importance of taking into consideration the dynamic evolution of the catalyst structure and composition are highlighted, focusing on findings extracted from in situ and operando characterizations. Additional theoretical insight into the reaction mechanisms underlying the improved C_{2+} selectivity of specific catalyst geometries and compositions in synergy with a well-chosen electrolyte are also provided.

Excessive CO_2 emissions from the utilization of traditional fossil energy sources cause severe environmental issues, hindering the sustainable development of our industrial society. The CO_2 electroreduction reaction (CO_2RR) represents a viable alternative to help close the anthropogenic carbon cycle and convert intermittent electricity from renewable energy sources (that is, solar and wind) to chemical energy in the form of fuels and feedstocks[1–3]. The most common products derived from CO_2RR are CO and formic acid. However, the production of more reduced products such as multicarbon oxygenates and hydrocarbons (C_{2+}) is highly desirable because of their higher energy density and wider applicability[4,5]. Such products are also of great significance from a point of view of fundamental research, since they involve the formation of the C–C bond, a key challenge in heterogeneous catalysis.

Extensive experimental and theoretical studies have focused on understanding the C–C coupling mechanism during the CO_2RR. Although the initial activation of the stable CO_2 molecule is difficult, the binding strength of an intermediate *CO (* being an adsorption site) and its subsequent conversion via proton-electron transfer into the next hydrogenated species (for example, *CHO, *COH, *OCCO or *OCCOH) on the catalyst surface determines whether H_2, CO or more reduced oxygenates and hydrocarbons are formed as final products[6,7]. For the formation of C_{2+} products, two pathways have been identified with regard to the C–C coupling step: (1) *CO dimerizes to form *OCCO species at low overpotentials[8], and (2) *CO is hydrogenated to form *CHO species[9], a common intermediate for the formation of methane, which takes place at high overpotentials. The first pathway was recently confirmed by an in situ spectroscopic observation of the hydrogenated CO dimer intermediate (*OCCOH) on the Cu(100) surface[10]. Differential electrochemical mass spectrometry (DEMS) measurements further revealed that acetaldehyde is an important intermediate for the formation of ethanol and propanol[11,12]. It should be noted that the C–C coupling step is highly sensitive to the structure of the catalyst and the electrolyte[13]. Cu is generally considered to be the only metal capable of producing hydrocarbons and oxygenates in significant amounts, but it still suffers from a high overpotential, low C_{2+}
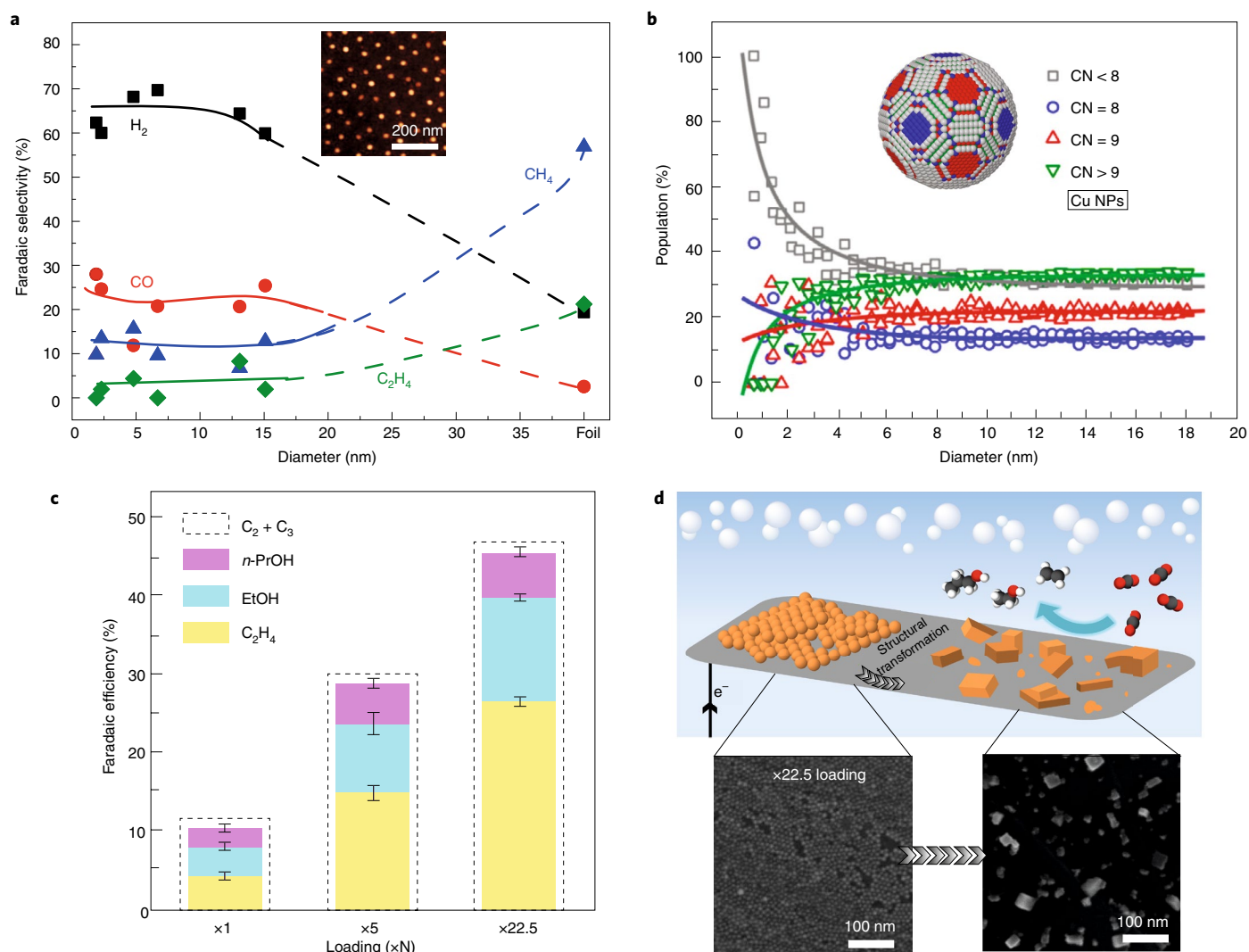
selectivity and a concurrent hydrogen evolution reaction (HER). To access C_{2+} products more efficiently, various nanostructured Cu catalysts have been developed by engineering low-coordinated sites and defects, tuning the oxidation state, adding a secondary metal or modifying the size and shape of nanostructures[14,15].

In this Review, we will discuss the current state-of-the-art Cu, Cu-bimetallic and some Cu-free catalysts towards the formation of C_{2+} products from the CO_2RR. The electrolyte effect on the catalyst structure before and during the reaction, as well as on the CO_2RR activity and selectivity, will also be discussed. Information extracted from in situ and operando characterization methods[16,17] will be used to shed light into the reaction mechanism and the dynamic evolution of the catalysts under CO_2RR conditions. Furthermore, the need of such studies in order to gain fundamental understanding of electrocatalytic processes will be prominently featured.

Catalyst design for C_{2+} products

Whether a catalyst can produce hydrocarbons and oxygenates, especially C_{2+} products via C–C coupling, essentially depends on its structure and composition. Nanostructured Cu-based materials are the most popular catalysts for C_{2+} products, while alternative non-Cu-based materials have also been explored. In this section, we review the recent advances made in the development of these state-of-the-art catalysts and their mechanistic understanding with special emphasis on the insights extracted from in situ and operando characterization methods.

Cu nanoparticles (NPs). Although Cu is an abundant and relatively cheap metal, maximizing the surface to volume ratio by using nanoparticulated catalysts is desirable for future implementation at the cathode of a CO_2 electrolyzer[18,19]. The special morphology of the NPs, together with their distinct electronic and chemical surface properties, usually confers improved catalytic activity compared to bulk materials. In this sense, the reactivity of NPs can be rationally tuned by modifying four fundamental parameters: size, shape, composition and interparticle distance (or loading on the support). The NP size determines the density of low-coordinated atoms present at

Department of Interface Science, Fritz Haber Institute of the Max Planck Society, Berlin, Germany. *e-mail: roldan@fhi-berlin.mpg.de

Fig. 1 | NP size and loading effects. a, Faradaic selectivity as a function of Cu NP size in a 0.1 M KHCO$_3$ electrolyte. The inset displays an AFM image of Cu NPs. **b**, Population of surface atoms with a specific coordination number as a function of the NP diameter with a schematic of a NP and its specifically coordinated surface atoms. **c**, Ethylene, ethanol and n-propanol FE selectivity as a function of the Cu NP loading, with the dotted lines showing the overall C$_2$–C$_3$ FE measured at −0.81 V versus RHE in a CO$_2$-saturated 0.1 M KHCO$_3$ electrolyte. **d**, Schematic and scanning electron microscopy (SEM) images illustrating the in situ transformation process of the Cu NP ensembles to cubic-like structures. Figures adapted with permission from: **a,b** ref. [20], American Chemical Society (2014) and **c–d** ref. [31], American National Academy of Sciences (2017).

its surface, which can influence the binding strength of the different reaction intermediates, and thus affect the final product selectivity. In this sense, a size-dependent study on Cu NPs showed an increased activity and enhanced selectivity towards H$_2$ and CO formation as the NP size decreased from 15 nm to 2 nm (Fig. 1a). The latter results were linked to a greater population of low coordinated sites in smaller NPs (Fig. 1b)[20] that favour HER versus CO$_2$RR. An analogous trend was also seen for Au (refs. [21,22]) and Zn (ref. [23]) NPs, and was theoretically explained as being due to the weaker binding of reaction intermediates such as COOH* to a NP surface covered by hydrogen[16].

Higher activity, and hydrocarbon and alcohol selectivity, have been described for gas diffusion electrodes (GDE) and membrane electrode assemblies (MEA), for example, those in which large NPs (25 nm) were deposited, resulting in a higher ethylene production (1148 μmol m^{-2} s^{-1}) with an exceptionally high Faradaic efficiency (FE, 92.8%) and suppression of the HER under galvanostatic conditions (j = 7.5 mA cm^{-2})[24]. These results bring into attention the importance of not only being able to fine-tune the catalytic material,

but also to the proper engineering of the different interfaces involved (gas–liquid–solid), for a better product selectivity at high current densities under practical reaction conditions. While catalyst integration into GDEs and MEAs is an emerging sub-field in CO$_2$RR[24,25], the integration of in situ and operando characterization methods coupled with the GDE and MEA configurations is difficult and rarely reported. To deal with this issue, one could learn from the in situ techniques and cells developed for applications in water electrolysis systems and fuel cells. An example of this are the X-ray absorption data acquired during real fuel cell and electrolyzer operation[26–29]. Nevertheless, the implementation of surface-sensitive techniques is still a challenge due to the relatively thick gas diffusion layer present in front of the active catalyst in the GDE configuration.

Adjusting the distribution of a catalyst on a support is another strategy that has been followed to further modify the CO$_2$ product selectivity. In this sense, Cu NPs with narrow NP size distribution and uniform arrangement demonstrated an increasing selectivity towards methane and ethylene as the interparticle distance decreased, which was assigned to an enhanced reactant

diffusion on the NP neighbourhood and the re-adsorption of intermediate species[30]. Nevertheless, local changes in the pH for different NP arrangements may also be partially responsible for the experimental results observed. The NP areal density was also found to be crucial for the observation of enhanced hydrocarbon selectivity[31,32] (Fig. 1c). In the former systems, the larger electroactive surface area available appears to facilitate the stabilization and reaction between different adsorbed reaction intermediates. It was postulated that this, accompanied by the limited mass transport at the catalytic surface, as well as the proton depletion and higher local interfacial pH, enables the selective conversion of CO_2 to C_2–C_3 hydrocarbons and oxygenates on highly packed Cu NP ensembles[31,32]. Interestingly, densely packed Cu NPs can undergo structural transformations during CO_2RR into electrocatalytically more active cube-like particles capable of forming ethylene, ethanol and n-propanol (Fig. 1d)[31]. These results highlight the consequence of the dynamic structural and compositional changes experienced by Cu-based catalysts during CO_2RR for the production of multicarbon products, and the need of cutting-edge characterization techniques based on in situ and operando microscopy and spectroscopy to further disentangle the parameters ruling the activity and selectivity of electrocatalysts.

Cu model surfaces. However, the wide surface heterogeneity of poly-oriented NPs makes difficult to extract clear correlations between the structural properties of the NPs and their reactivity. The use of model surfaces can serve to overcome this problem by being able to more directly extract information on the effect of surface structure on a given electrocatalytic reaction pathway. Accordingly, control over selectivity can be achieved by maximizing the exposure of the facets that have been previously proven more reactive for a certain process. Regarding CO_2RR, preceding studies using Cu single crystals have shown that ethylene is selectively formed on Cu(100), while Cu(111) favours the formation of methane[33,34]. The presence of surface defects such as steps or kinks (that is, under-coordinated sites) on a well-ordered surface may also enhance the activity by modifying the surface binding energy of the adsorbates, thus changing the reaction pathway towards different products[35,36]. Theoretical studies, although still in an incipient stage due to the challenges associated with properly treating a complex electrode–electrolyte interface, have also devoted significant effort to unravelling the mechanism behind the different product selectivity on each surface orientation[8,35,37,38]. The most accepted theory so far proposed that the reaction pathway that yields to ethylene formation takes place via CO dimerization in a proton-decoupled one-electron reaction step, generating a $C_2O_2^-$ intermediate that is subsequently protonated[8,38]. In addition, the atomic square configuration of the Cu atoms on a (100) surface presents an optimal adsorption geometry for this dimer, and a better stabilization of the charged intermediate[38]. Later in situ experimental spectroscopic studies have revealed a hydrogenated CO dimer intermediate during CO electroreduction on Cu(100) (Fig. 2a)[10], and also found that high surface coverage of adsorbed *CO is essential for the selective formation of ethylene[34]. Furthermore, the dynamic changes of the surfaces, even in the case of single crystals under reaction conditions must be considered. Recent quasi-operando electrochemical scanning tunnelling microscopy (EC-STM) and DEMS measurements demonstrated the transformation underwent by a Cu(polycrystalline)–Cu(100) reconstructed surface when subjected to oxidation–reduction cycles in a 0.1 M KOH solution[39]. The resulting ordered stepped surface, Cu(S)–[3(100)×(111)] or Cu(511) was found to reduce CO to ethanol at a lower overpotential and higher rate than the pristine Cu(100) surface. These results are in agreement with previous studies that reported the beneficial effect of (111) and (110) steps in (100) facets for the C–C bond formation[33,40].

Shape-controlled Cu nanocatalysts. The surface structure sensitivity of the CO_2RR, together with the aforementioned theoretical considerations, hints towards the advantage of using NPs with controlled morphology to explore the so-called facet effect and prepare tailored materials with superior activity and selectivity. For example, by synthesizing cubic-shaped Cu nanostructures it is possible to guarantee the presence of well-ordered (100) domains while preserving the characteristic low-coordinated sites from NPs, morphology that has been demonstrated to lead to an increased ethylene selectivity and suppressed methane production[41–43], especially when combined with Cu^+ and subsurface oxygen species[44]. The main drawback of these shape-selected nanocatalysts is their deactivation due to the loss of the well-defined facets and decrease in size under reaction conditions[35]. For instance, lower selectivity towards ethylene and ethanol in favour of methane production was found after the disappearance of the (100) facets on Cu nanocubes deposited on carbon (Fig. 2b)[45]. In this study, in situ and operando techniques such as electrochemical atomic force microscopy (EC-AFM), X-ray absorption fine-structure spectroscopy (XAFS) and quasi in situ X-ray photoelectron spectroscopy (XPS) were crucial to correlate the changes in activity with the dynamic surface roughening, defect and pore formation, and CuO_x reduction of the Cu nanocubes. Moreover, the lack of stability of Cu^+ species on the Cu cubes supported on carbon, as compared to those grown on a Cu foil, was also held responsible for the switch in the reaction selectivity from C_2H_4 for Cu cubes grown on Cu to CH_4 for those deposited on carbon.

Other singular morphologies like highly porous 3D Cu dendrites and foams[46–49] have also shown high CO_2RR activity and enhanced ethylene selectivity. However, since no preferential facet orientation prevails on these nanostructured materials, the high density of defects (steps, kinks and edges)[50], grain boundaries[51] and surface roughness[46,52], together with the concomitant changes in the interfacial pH[53], are considered to be the parameters determining the resulting catalytic behaviour. The residence time of the intermediates inside these 3D catalysts appears to be crucial for the C_2 product selectivity, as it was previously pointed out for ensembles of densely packed Cu NPs.

Oxide-derived Cu (OD-Cu) catalysts. Cu metal nanostructured surfaces derived from the in situ reduction of highly oxidized materials under CO_2RR conditions also present unprecedented catalytic activity[54], namely, lower onset potentials and enhanced selectivity toward C_{2+} products over methane. Such trends have been assigned to their rough morphology and large defect density, also leading to changes in the local pH, as well as to possible changes of the chemical state of the active Cu species. In this sense, CO_2RR has been lately studied on OD-Cu surfaces with different morphologies (nanoneedles, nanocrystals and NPs) using operando selected-ion flow tube mass spectrometry (SIFT-MS), and in situ Raman spectroscopy[55]. The results indicate that the reduction of Cu_2O is energetically and kinetically favoured compared to CO_2RR, thus taking place before the selective generation of C_2 products[45]. Similar conclusions were extracted from the ex situ study of [18]O isotopically enriched OD-Cu catalysts, where the residual [18]O content found after CO_2RR was negligable[56]. However, recent reports have suggested that Cu^+ and residual subsurface oxygen might be at least partially responsible for the outstanding activity of OD-Cu catalysts[27,57–60]. According to theoretical simulations, the kinetics and thermodynamics of both CO_2 activation and CO dimerization significantly improve due to the presence of subsurface oxygen[58] and Cu^+ and Cu^0 species at neighbouring surface sites[59], thereby increasing the efficiency and selectivity of CO_2RR. Due to the rapid reoxidation of oxide-derived materials, the accuracy of ex situ measurements to determine the oxygen content is jeopardized, and in situ and operando methods are required. Experimental evidence of the survival of Cu^+ species
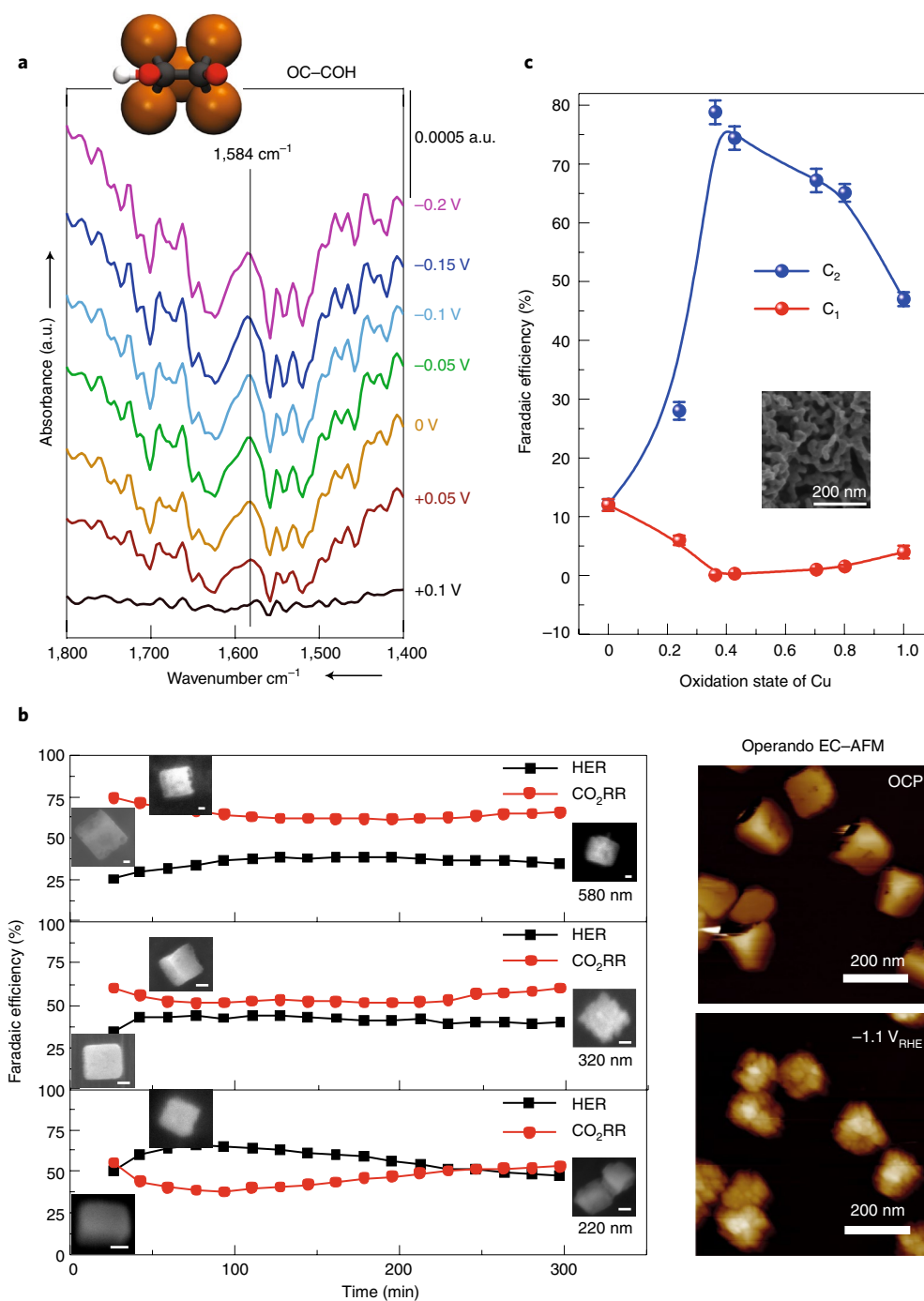
Fig. 2 | Real time characterization of Cu-based catalysts. a, Potential dependent absorbance spectra for Cu(100) in a 0.1 M LiOH solution using D_2O as electrolyte. The highlighted band at 1584 cm⁻¹ corresponds to ¹²C=O stretching from the adsorbed hydrogenated CO dimer (OCCOH) intermediate, as depicted in the schematic structure. **b**, Faradaic efficiency for CO_2RR and HER of samples with different Cu cube sizes (580 nm, 320 nm and 220 nm) recorded at −1.05 V versus RHE over 5 hours. The insets display SEM images of Cu cubes measured after different reaction times. The size of the scale bars is 100 nm. Operando EC-AFM images of ~100 nm large Cu cubes acquired in 0.1 M $KHCO_3$ at open circuit potential (OCP) and at −1.1 V versus RHE for 1 min. **c**, Faradaic efficiency of C_2 and C_1 products obtained from Cu(B) samples with different Cu oxidation states tested at −1.1 V versus RHE. The inset displays an SEM image of this material. Figures adapted with permission from: **a** ref. [10], Wiley (2017); **b** ref. [45], Wiley (2018) and **c** ref. [60], Nature Publishing Group (2018).

during CO_2RR was provided on plasma-oxidized Cu catalysts based on operando XAFS measurements. Interestingly, these catalysts displayed a high ethylene selectivity of 60% at −0.9 V versus RHE[57]. The stabilization of Cu⁺ has been recently achieved at interfaces between Cu cubes and a Cu foil[44,45], on CuO_x foils by adding I⁻ to the electrolyte[61,62], and on porous dendritic nanostructures by using

boron as a dopant (Cu(B)) to modify the electronic structure of Cu. In the latter example, a conversion to C_2 products of up to 80% FE at −1.1 V versus RHE and 40 hours of initial sustained efficient operation (Fig. 2c)[60] was reported. While one cannot neglect the role of the increased electrochemically active surface area (ECSA) of the highly roughened Cu catalysts in the reactivity trends obtained,

the intrinsic activity cannot be simply determined by normalizing the current density by the ECSA[63,64]. In fact, such an approach fails to consider the complexity of the catalytically active surface sites, which are not homogenous in nature. Therefore, it cannot be expected that every surface site would display an identical catalytic performance. It is well known in heterogeneous catalysis[65] that this is in fact not the case, and that at times, only a few surface sites dominate the catalytic activity and selectivity trends. Nevertheless, in order to rule out the effect of the ECSA in CO_2RR, control experiments should be conducted on samples with similar ECSA but where distinct active surface features (for example, specific defects) are present[44,57]. Although the catalytic effect of Cu^+ and subsurface oxygen in Cu-based materials is a current topic of debate in electrocatalysis[66], these results are promising and pave a way to finely tune the properties of Cu towards higher activity and narrower product distribution.

Cu-based bimetallic catalysts. The formation of bimetallic alloys of Cu with various secondary metals is commonly used to alter the activity and selectivity of CO_2RR. The catalytic performance of bimetallic catalysts for CO_2RR varies as a function of their surface composition and structure, both of which might be modified during CO_2RR. For instance, even when the same initial bimetallic composition is chosen (for example, CuPd bimetallic catalysts)[67–70], different products may be produced according to subtle changes in one of the former parameters under reaction conditions.

It is generally assumed that the distinct activity and selectivity for CO_2RR of bimetallic alloy catalysts might be assigned to changes in their electronic and geometric structure originating from the modification of the interatomic distance of surface atoms brought about by the incorporation of a different atom in the lattice[71,72]. These changes lead to strain, and altered binding strengths of reaction intermediates, by shifting the centre of the electronic d-band. Such effects have been demonstrated for Cu overlayers on Pt (ref. [73]), where CH_4 production was found to increase with increasing film thickness under tensile strain. Core-shell bimetallic structures with an inexpensive core are also of interest for CO_2RR, especially in cases where ultrathin Cu layers can be stabilized at the NP surface on other metals that would lead to expansive lattice strain, since under such conditions a more favourable stabilization of the reaction intermediates has been predicted[74].

The reaction selectivity has also been shown to be strongly dependent on the composition of the bimetallic system. For example, for bimetallic AuCu NPs, Kim et al.[75] described increased CO production with increasing Au content, with the optimal Au_3Cu composition leading to a mass activity exceeding 200 A g^{-1} at -0.73 V versus RHE. However, the distinct CO selectivity could not be exclusively assigned to changes in the electronic structure (Fig. 3a), due to the similarities observed for pure Au and Au_3Cu. Instead, synergetic electronic and geometric effects had to be invoked for the AuCu NPs in order to understand their altered activity for CO_2RR through the modification of the intermediate binding strength (Fig. 3b). Similar results were found by Li et al.[70] for mesoporous PdCu with Pd_7Cu_3 exhibiting the highest activity for CO production with over 80% FE. Based on density functional theory (DFT) calculations, Pd atoms were found to act as reactive centres and promote CO desorption by altering the electronic structure of Cu at neighbouring Pd sites, increasing the CO_2 to CO selectivity. Along these lines, distinct selectivity trends were reported for PdCu NPs with ordered, disordered and phase-separated atomic arrangements (Fig. 3c)[68]. In particular, phase-separated PdCu NPs exhibited high selectivity for C_2 products (>60% FE), while an ordered PdCu catalyst generated C_1 products (>80% FE). The degree of intra-particle atomic ordering was also shown to control the selectivity of AuCu NPs (Fig. 3d)[76], with disordered AuCu NPs favouring H_2 production while ordered AuCu NPs favoured CO_2 to CO conversion. These results highlight that the atomic ordering of the metal constituents in bimetallic catalysts plays an important role in determining the catalytic selectivity. Surface segregation of one of the bimetallic components under CO_2RR reaction conditions should also be taken into consideration. For example, for small size-controlled AuCu catalysts, Au surface segregation was found to lead to an increase in CO selectivity at the expense of hydrocarbons[22]. Direct evidence of the surface segregation phenomena was also reported via quasi in situ XPS and operando XAS for CoCu catalysts, which revealed Cu surface segregation under reaction conditions (Fig. 3d)[74]. Nevertheless, in both cases due to the small size of the NPs (below 5 nm), the large number of under-coordinated surface sites and the compressive strain of the Cu lattice at the NP shell (due to the Co core), CO and H_2 selectivity instead of multicarbon selectivity, was favoured.

The use of co-catalysts has also been proposed as a viable alternative to enhance multicarbon product generation by contributing CO-producing sites that facilitate reaction pathways involving *CO intermediates. One notable example is the work of Ren et al. on oxide-derived Cu–Zn catalysts[77], which demonstrated enhanced C_2H_5OH production (29% FE, -8.2 mA cm^{-2} at -1.05 V versus RHE) for a Cu_4Zn composition. Operando Raman spectroscopy data revealed that CO was adsorbed on Cu sites only, and this was postulated to originate from the spillover of CO from the Zn to the Cu site, and deemed crucial for the formation of C_2H_5OH at the Cu surface (Fig. 3e). Subsequently, the combined effects of CO spillover and atomic ordering were proposed by Lee et al. for phase-separated and phase-blended Ag–Cu_2O electrodes[78]. Incorporating Ag into Cu_2O was shown to result in higher C_2H_5OH production as compared to pure Cu_2O, which was also assigned to an increase in CO population arising from the Ag sites. Moreover, the phase-blended Ag–Cu_2O catalyst showed higher ethanol selectivity than phase-separated Ag–Cu_2O, even though the Ag content on the surface of the phase-separated Ag–Cu_2O electrode was reported to be larger. It was proposed that an optimum distribution and distance between the Ag and Cu atoms was important in order to facilitate efficient CO transfer from Ag to Cu sites, thus enhancing the product selectivity toward ethanol.

The reactivity of bimetallic catalysts for CO_2RR is affected by a variety of factors that must be considered for their rational design. Based on the literature[22,67–83], it seems that the modification of the intra-particle atomic arrangement and spillover effects must be considered in order to develop bimetallic catalysts able to generate C_{2+} products. However, it should also be noted that the majority of the previous studies are based on experimental data acquired from the as-prepared samples, not considering that the surface composition and chemical state of the catalyst may change during the reaction. In the future, additional attention needs to be dedicated to the implementation and use of in situ and operando techniques (for example, XAFS, XPS and liquid-TEM) in order to gain in depth information on the dynamic behaviour of the structure and composition of CO_2RR electrocatalysts.

Non-Cu catalysts. A key descriptor that allows Cu to produce hydrocarbons and alcohols is the moderate binding strength of the CO intermediate. Therefore, it might be possible to get a comparable CO binding strength by combining a metal that binds CO strongly with another that binds CO weakly. For example, a Pd-modified Au electrode was reported to be able to reduce CO_2 to C_1–C_5 hydrocarbons[84]. This strategy was also applied to non-noble metals, such as NiGa (ref. [85]) and NiAl (ref. [86]). However, these catalysts still showed very poor selectivity (<5% FE) toward hydrocarbons[84,85] and alcohols[86]. In general, nanostructuring metal surfaces will induce the formation of defects and low-coordinated sites, which could bind CO stronger compared to their bulk counterparts[87]. This significant change of the surface coordination might transform a CO-producing catalyst (weak CO binding) into a hydrocarbon- and
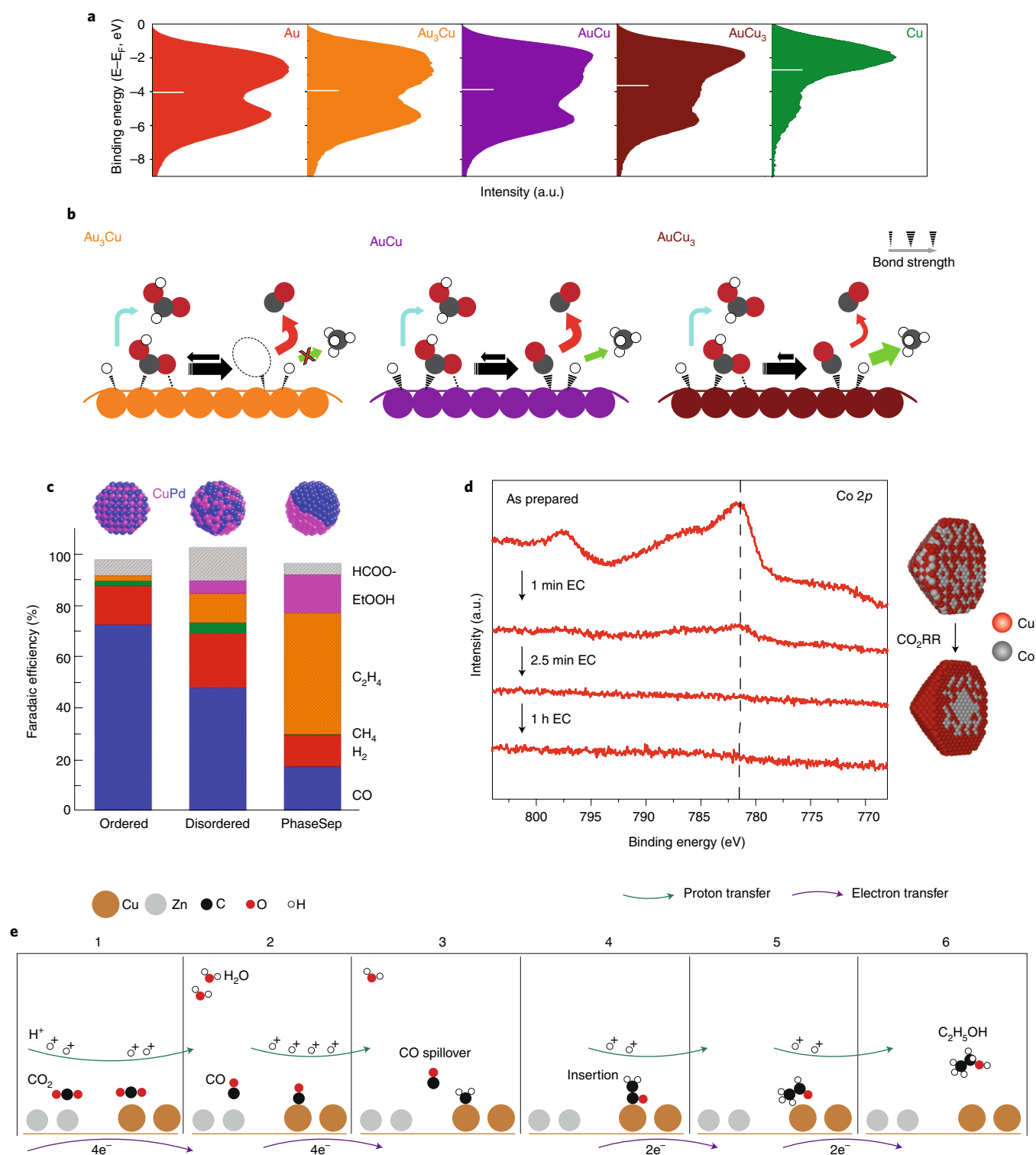
Fig. 3 | Various parameters affecting the CO$_2$RR selectivity of Cu-based bimetallic catalysts. a, Surface valence band photoemission spectra of AuCu bimetallic NPs. The white bar indicates the centre of the d-band. **b**, CO$_2$RR mechanism for AuCu bimetallic NPs describing changes in the binding of reaction intermediates. **c**, FEs of PdCu NPs with different mixing patterns. **d**, Quasi in situ XPS spectra of the Co 2p core level region of CoCu NPs as a function of various CO$_2$ electroreduction times at −1.1 V versus RHE. Model representation for surface segregation of CoCu NPs under CO$_2$RR. **e**, Proposed mechanism for CO$_2$RR to C$_2$H$_5$OH on Cu$_x$Zn catalysts. Figures adapted with permission from: **a,b** ref. [75], Nature Publishing Group (2014); **c** ref. [68], American Chemical Society (2017); **d** ref. [74], Elsevier (2018) and **e** ref. [77], American Chemical Society (2016).

alcohol-producing catalyst. Nevertheless, it should be considered that when the size of the electrocatalyst is further reduced, and very high populations of under-coordinated atoms are present, a

stronger H-binding (competing HER) would result in a weakening of the CO binding and a switch in the selectivity from CO to H$_2$, as was observed before for Au NPs (ref. [21]) and Zn NPs (ref. [23]) below
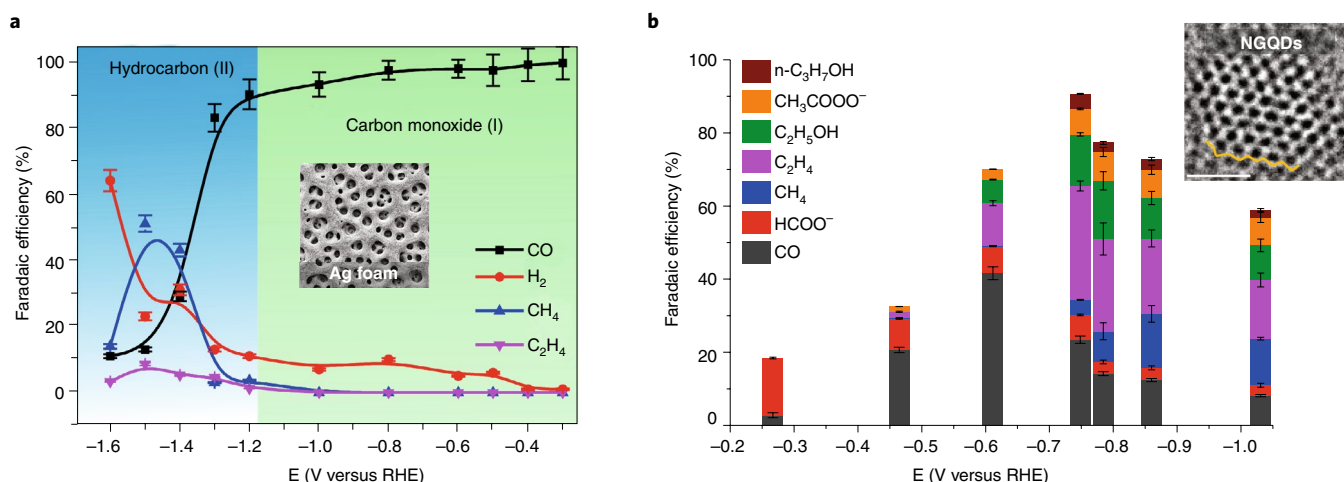
Fig. 4 | Non-Cu catalysts for the production of hydrocarbons and oxygenates. a,b, Potential-dependent FEs of CO_2RR products over an Ag foam catalyst (**a**) and N-doped graphene quantum dots (NGQDs) (**b**). The insert in (**a**) displays a SEM image of the Ag foam and the insert in (**b**) displays a TEM image of a single NGQD containing a zigzag edge (outlined by a yellow line). Figures adapted with permission from: **a** ref. [88], American Chemical Society (2018) and **b** ref. [101], Nature Publishing Group (2016).

8 nm. Nonetheless, highly porous Ag foam catalysts demonstrated a ~60% FE toward methane and ethylene at −1.5 V versus RHE (Fig. 4a)[88]. This remarkable Cu-like behaviour was rationalized in terms of the significantly increased CO binding energy of the mesoporous Ag foam. This phenomenon, observed at very high overpotentials, may inspire researchers to re-think the catalytic performance of other highly defective nanostructured Ag catalysts that usually produce only CO at low overpotentials[89]. Furthermore, when the early transition metals, such as Mo, W, Ta, Fe and Ti (strong CO binding), are converted to carbides, the binding energy of CO was found to become weaker due to the more carbophobic and oxophilic nature of these carbides[90]. For instance, Mo_2C could reduce CO_2 to methane at lower overpotentials (−0.55 V to −0.8 V versus RHE) than Cu, although with a very low efficiency (<0.1% FE)[91]. Transition metal chalcogenides have been theoretically predicted to be active for CO_2RR (ref. [92]), and MoS_2 was reported to reduce CO_2 to n-propanol (~3.5% FE) in 0.1 M $NaHCO_3$ (ref. [93]). However, the selectivity toward hydrocarbons and alcohols was severely suppressed due to the more favourable hydrogen evolution pathway on the carbide and chalcogenide catalysts in aqueous electrolytes. Recently, nickel phosphide (Ni_2P) was reported to selectively reduce CO_2 to C_3 and C_4 products at overpotentials as low as 10 mV (for example, 71% FE for 2,3-furandiol at 0 V versus RHE), but the current density was quite low (<0.5 mA cm^{-2}) (ref. [94]).

Theoretical predictions have indicated that single-atom catalysts with an active metal atom embedded either in another metal (nitride or carbide)[95,96] or in a nitrogen-doped carbon matrix[97,98] also have the potential to reduce CO_2 to higher products beyond CO and formate. Single-Ir-doped TiC (Ir@TiC) was found to have a remarkably low overpotential of −0.09 V for the selective production of methane[95]. Cheng et al.[96] theoretically studied a series of single-atom alloys with the major component being either gold or silver in combination with isolated single atoms (Rh, Ir, Cu, Ni, Pd, Pt and Co) replacing surface atoms, and found Rh@Au(100) and Rh@Ag(100) to be the most active combinations for methane formation. Theoretical investigations of single transition metal atoms anchored on defective graphene with single or double vacancies (M@sv-Gr; M@dv-Gr, respectively) revealed Ni@dv-Gr and Pt@dv-Gr as promising materials for methanol production, and Os@dv-Gr and Ru@dv-Gr for methane production[97]. While these theoretical studies showed great potential, significant production of hydrocarbons or alcohols on realistic single atom catalysts still needs to be experi-

mentally demonstrated. Recently, Ju et al.[98] reported high CO selectivity (85% FE) for metal- and nitrogen-doped porous carbons with porphyrin-like C–N structures (M–N–C, M = Mn, Fe, Co, Ni or Cu). In addition, Mn–N–C and Fe–N–C were also found to produce trace amounts of methane (<0.5% FE), which was assigned to the stronger CO binding of the Fe and Mn porphyrine-like structures[99]. The selective production of acetic acid (61% FE at −0.5 V versus Ag/AgCl) over ferrihydrite-like (Fh-FeOOH) clusters supported on N-doped carbon was also reported[100]. Here the reactivity was correlated to the formation of nitrogen-coordinated iron (II) sites as single atoms or polyatomic species at the interface between iron oxyhydroxide and the nitrogen-doped carbon, and to the N species acting concertedly to enable the C–C coupling.

The role of N or N–C species in C–C formation during CO_2RR was further described in metal-free carbon materials[101–105]. N-doped graphene quantum dots (NGQDs) showed an ~55% FE for multicarbon products and partial current densities of 46 and 21 mA cm^{-2} for ethylene and ethanol at −0.86 V versus RHE respectively, which is comparable to those obtained with Cu NPs catalysts (Fig. 4b)[101]. The fact that GQDs primarily yielded CO and formate demonstrated the decisive role of the pyridinic N species at the utmost exposed edge sites of NGQDs in the C–C formation. Furthermore, N-doped nanodiamond showed a ~77% FE for acetic acid between −0.8 and −1.0 V versus RHE, resulting from its high hydrogen evolution potential and N-doping, where N–sp^3C could be the most active species[102]. Boron- and nitrogen-co-doped diamond surprisingly reduced CO_2 to ethanol with 93.2% FE at −1.0 V versus RHE[103], while the B-doped diamond mainly produced formaldehyde[103,104]. The high ethanol selectivity could be attributed to the synergetic effect of B and N co-doping and the fine balance between N content and hydrogen evolution potential. However, the change in the reaction pathway leading to a selectivity switch for the main products from acetic acid to formaldehyde and ethanol as a function of the different dopants still needs to be experimentally and theoretically clarified.

Electrolyte design for C_{2+} products

The role of the electrolyte cannot be neglected in an electrochemical reaction, since it will participate in the reaction through its interaction with the electrode surface as well as the reactants, intermediates and products. Understanding these effects on the catalyst structure and the reactivity will help improve the CO_2RR activity and C_{2+} selectivity via rational electrolyte design.
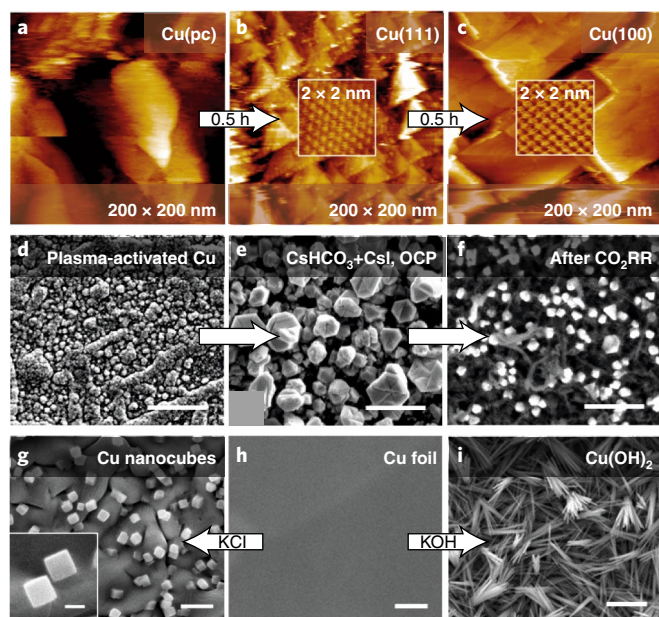
Fig. 5 | Electrolyte effect on catalyst structure. a–c, EC-STM images of polycrystalline Cu acquired under CO_2RR at −0.90 V (versus SHE) in 0.1 M KOH after different reaction times. **d–f**, SEM images displaying the surface morphology of an O_2-plasma-oxidized Cu foil (**d**), and after immersion in $CsHCO_3$+CsI at open circuit potential (OCP, **e**) and after 1 hour of CO_2RR at −1.0 V versus RHE (**f**). All the scale bars are 5 μm. **g–i**, Electrolyte-driven nanostructuring of a pristine metallic Cu foil (**h**; scale bar, 2 μm) and a similar foil after cycling in KCl (**g**; scale bars, 2 μm (image) and 200 nm (insert)) and in KOH (**i**; scale bar, 5 μm). Figures adapted with permission from: **a–c** ref. [108], Springer Nature Ltd (2014); **d** ref. [61], American Chemical Society (2017); **e,f**, ref. [62], American Chemical Society (2018); **g,h** ref. [44], American Chemical Society (2017) and **i** ref. [110], American Chemical Society (2018).

Electrolyte effect on catalyst structure. It has been shown that CO_2RR is very sensitive to the structure of the electrode and therefore the dynamic processes that electrodes may undergo upon exposure to the electrolyte and applied potential must be considered. Thorough spectroscopic and microscopy characterization, before, after, but even more importantly, under operando reaction conditions, are key to understanding the real nature of the catalytically active sites[45,88,106]. For instance, a polycrystalline Cu electrode surface was found via EC-STM to undergo a significant surface reconstruction during CO_2RR in 0.1 M $KHCO_3$ from a polycrystalline surface to a well-known ethylene-selective Cu(100) surface orientation within 3 hours at −0.9 V versus SHE (ref. [107]). This transformation became faster in 0.1 M KOH and had a transition stage with Cu(111) as intermediate orientation (Fig. 5a–c)[108]. Nevertheless, no information could be found in the former literature regarding a possible change in the selectivity of this catalyst with reaction time. Recently, operando EC-AFM measurements revealed that carbon-supported Cu nanocubes lose their cubic shape and decrease in size during CO_2RR in 0.1 M $KHCO_3$, and the morphology change was found to correlate with time-dependent activity and selectivity changes (Fig. 2b)[45].

Plasma-oxidized Cu foil catalysts with excellent C_{2+} selectivity were found to form shaped CuI particles on the surface in I⁻-containing electrolytes even at open circuit potential (OCP), and the morphology of the shaped particles could be tuned by introducing different cations (K⁺ versus Cs⁺) in the electrolyte (Fig. 5d–f)[61,62]. Remarkably, the electrolyte pre-restructured catalyst surfaces underwent different changes during CO_2RR. The CuI crystals

were reduced to form a highly porous surface in the KI-containing electrolyte, while in the CsI-containing electrolyte some smaller CuI particles survived during the reaction, which helped to stabilize Cu⁺ species that were found to facilitate C–C coupling[59]. The larger cations (Cs⁺ versus K⁺) contributed more favourably to the stabilization of the CuI species.

Inspired by the dynamic evolution of catalyst structures induced by the electrolyte and the applied potential, an electrolyte-driven nanostructuring strategy was applied to synthesize efficient CO_2RR catalysts. By cycling an electropolished Cu foil in a KCl solution, well-defined Cu nanocubes (Fig. 5g)[44] could be grown on the surface with sizes that could be tuned by changing the KCl concentration. In combination with low-pressure O_2 plasma pre-activation, these Cu nanocube catalysts showed a vastly improved selectivity (73% FE) toward C_2–C_3 hydrocarbons and alcohols[44]. This synthesis method ensured well-defined Cu(100) facets in the as-prepared samples and also improved morphological stability during CO_2RR, compared to related systems prepared by the metal ion battery cycling method[109] or in situ generated in a KCl-containing $KHCO_3$ solution[42]. Other halide salts (KBr, KI) were also used to modify the Cu surface and showed high C_{2+} selectivity. Moreover, when a polycrystalline Cu foil was electrochemically oxidized in concentrated KOH by an anodization process, $Cu(OH)_2$ nanowires (Fig. 5i)[110] were grown on the surface, which were further reduced to a Cu catalyst with mixed oxidation states under reaction conditions. These examples show the rich possibilities for the design of new catalysts via electrolyte-driven nanostructuring.

Electrolyte effect on CO_2RR reactivity. Apart from the obvious effect on the catalyst structure, electrolytes also play an important chemical role in the CO_2RR. Understanding mechanistically the electrolyte effect would help improve the activity and selectivity of CO_2RR via efficient electrolyte design. The size of alkali metal cations was shown to strongly affect the product distribution over Cu-based catalysts and the presence of larger cations (for example, K and Cs) facilitated the formation of C_{2+} products over both metallic Cu[111–113] and CuO_x[62] catalysts (Fig. 6a,b). The effect of alkali metal cations on the reaction pathways is still under debate. Singh et al.[111] theoretically interpreted the effect by preferential cation hydrolysis in the vicinity of the electrode and proposed that the stronger buffering effect of larger cations lowered the local pH near the electrode, leading to higher local CO_2 concentration. This hypothesis was verified experimentally by probing the pH at the electrode–electrolyte interface using in situ surface-enhanced infrared absorption spectroscopy and operando Raman spectroscopy[49,114]. DFT calculations revealed that the intermediates toward C_{2+} formation were stabilized by the electrostatic interactions between solvated cations at the outer Helmholtz plane (OHP) and adsorbed species with large dipole moments[112]. While cations only populated the OHP in these studies over metallic Cu surfaces[96], a recent study from Gao et al.[62] revealed that the solvated cations can be specifically adsorbed on both metallic and pre-oxidized Cu electrode surfaces under CO_2RR conditions when the explicit surface solvation around the adsorbed cation is considered. Following the same DFT-based modelling method, subsurface oxygen was found to promote the specific adsorption of cations and accentuated the effect of the cations, significantly promoting CO* formation (one of the intermediates toward C_{2+}) (Fig. 6c; ref. [62]). In addition to the alkali metal cations, the presence of multivalent cations can also accelerate CO_2RR rate and influence the product selectivity. On a CuSnPb alloy electrode[115], the CO_2RR rate in a La^{3+}-containing acidic electrolyte was two times higher than that in Na⁺ at the same potential, and in the presence of Zr^{4+}, CH_3CHO (17.6% FE) was produced, and CH_3OH (35% FE) and HCOOH (28% FE) were produced in the presence of Na⁺. However, the application of multivalent cations was limited by their low solubility.
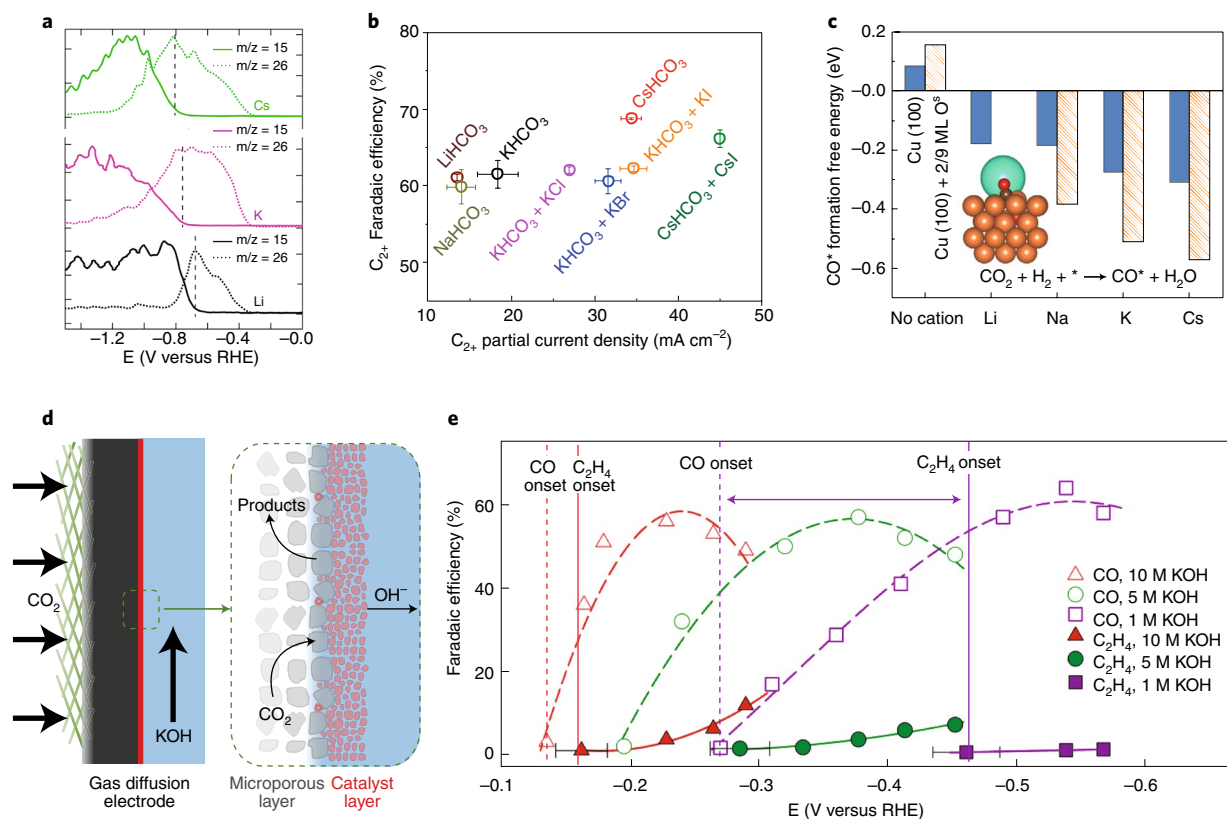
Fig. 6 | Electrolyte effect on CO₂RR reactivity. a, DEMS mass fragments associated with the reduction products formed during CO reduction on a Cu(100) electrode in different 0.1 M alkaline hydroxide solutions. **b**, FEs and partial current densities of C_{2+} products obtained from a plasma-oxidized Cu foil catalyst in different electrolytes after 1 hour of CO₂RR at −1.0 V versus RHE. **c**, CO* formation free energy calculated in the absence and presence of Li*, Na*, K* and Cs* on bare Cu(100) and Cu(100) with 2/9 ML subsurface oxygen (O^s). **d**, Schematic of the cathode portion of a gas diffusion electrode (GDE) for CO₂RR. **e**, C_2H_4 and CO FEs of a Cu GDE in KOH with different concentrations. Figures adapted with permission from: **a** ref. [113], American Chemical Society (2017); **c** ref. [62], American Chemical Society (2018) and **d,e** ref. [19], American Association for the Advancement of Science (2018). Data in panel b are from refs. [61,62].

Aqueous solutions of bicarbonate salts, rather than other anions (for example, SO_4^{2-}, ClO_4^-), are generally used as the electrolyte for CO₂RR since a higher effective CO₂ concentration near the electrode surface is accessible through a rapid equilibrium between bicarbonate and the dissolved CO₂ molecule, as observed by operando FTIR[116–118]. In combination with the presence of halides in the bicarbonate electrolyte, the formation of C_{2+} products over plasma-oxidized Cu catalysts was significantly increased (Fig. 6b)[61,62], which was attributed to the specific adsorption of halides with a higher coverage on the pre-oxidized Cu surface during the reaction (as shown in Fig. 5d–f)[61,62]. However, in contrast to the metallic Cu foil, when a metallic Cu (100) single crystal electrode[119] was measured in pure potassium halide electrolytes, the formation of ethylene and ethanol increased from Cl^- to Br^- to I^-. The specifically adsorbed halides could participate in the initial activation of CO₂ as well as the further hydrogenation through a strong interaction with the adsorbed intermediates[61,62,119–121].

To minimize the competing HER, a higher electrolyte pH (the concentration of H^+ or OH^-) is preferred. Meanwhile, higher (local) pH also favours the formation of ethylene over methane[52,122]. However due to the acidic nature of the CO₂ molecule, a strong alkaline electrolyte cannot be achieved in a regular H-type electrochemical cell[18]. The gas diffusion electrode configuration (GDE, Fig. 6d)[19] used in a flow cell, with concentrated KOH instead of KHCO₃ as the electrolyte, makes the strong alkalinity possible and provided the benefit of diffusion of CO₂ across the gas–liquid interface. By increasing the KOH concentration from 1 M to 10 M,

ethylene started to evolve over a Cu GDE at only −0.165 V versus RHE, almost simultaneously with the CO production (Fig. 6e)[19]. Similarly, Jouny et al.[123] reported CO electroreduction over oxide-derived Cu catalysts in a flow cell with a C_{2+} FE of 91% and 630 mA cm^{-2} at −0.67 V versus RHE, which pushed closer the CO₂RR to future industrial applications. However, the challenge remains regarding how to increase the commercially relevant long-term stability of catalysts in the GDE configuration while maintaining the initial high activity and C_{2+} selectivity.

The finite CO₂ solubility in water (33 mM at 25 °C, 1 atm) leads to an upper diffusion-limited CO₂RR rate. Although one could bypass this issue by using the GDE configuration, increasing the CO₂ pressure (to even supercritical conditions) would also increase the CO₂ concentration in aqueous electrolytes[124,125]. Nevertheless, further efforts are still needed to address critical issues arising from the high-pressure configuration, such as the corrosion of the Cu electrodes and the formation of carbon deposits. Compared to water, some organic solvents (for example, acetonitrile, methanol and N,N-dimethylformamide) and ionic liquids have a several-fold higher CO₂ solubility and can be used as an alternative reaction medium. In addition to being a solvent, an ionic liquid can also serve as a co-catalyst in the aqueous electrolyte due to its ability to complex with CO₂, which lowers the energy of the initial reduction barrier[126]. For example, a Cu(I) and carbon-doped boron nitride composite catalyst reduced CO₂ to acetic acid with 80.3% FE when a 1-ethyl-3-methylimidazolium tetrafluoroborate ([Emim]BF₄)-LiI-water solution was used as the electrolyte[127].

Summary and outlook

As discussed in this Review, the CO_2RR over a real complex catalyst is controlled by multiple factors including surface roughness, defect density, nanoparticle size, shape, composition, interparticle distance and the electrolyte[13]. In order to disentangle their relative contributions, further investigations on morphologically and chemically well-defined model catalysts are required. The fundamental knowledge that can be gained from the former systems can be used to create an optimum catalyst configuration leading to a given desired activity and selectivity. Furthermore, most of the current studies focusing on facilitating C–C coupling were conducted on metallic Cu systems. Additional work on other relevant model materials including Cu alloys, segregated Cu-bimetallic systems and active non-Cu-based systems should be further developed.

The application of in situ and operando characterization techniques in CO_2RR studies is highly desirable, since we have learned that the insights from those characterization techniques do help the rational design of efficient catalysts and electrolytes. For example, we reported the positive correlation between ethylene formation and the presence of Cu^+ species based on an operando XAFS study[57], followed by the quasi in situ XPS work[44,45], correlating the selectivity for C_{2+} products to the content of Cu^+ species stabilized on Cu nanocubes after O_2-plasma pre-treatments, as well as at interfaces between Cu cubes and Cu substrates. Later on, the role of halides and cations in the electrolyte in the stability of Cu^+ (for example, as CuI) and subsurface oxygen species[61,62] was also discussed, and a correlation found with C_{2+} selectivity. Such findings were subsequently used in the design of Cu catalysts by other groups[60]. These important advances clearly show the crucial role of in situ and operando techniques in electrocatalysis studies.

By rational design of catalytic electrodes and electrolytes, improved selectivity and C_{2+} production rate from the CO_2RR could be achieved. The use of a gas diffusion electrode configuration is already helping to close the gap between laboratory discovery and industrial needs, achieving over 80% FE for C_{2+} and >0.5 A cm^{-2} partial current density at reasonable overpotentials[19,123]. However, the long-term stability of these catalysts at such high activity and selectivity still poses a significant challenge. Furthermore, the selectivity towards a specific C_{2+} product (for example, ethylene) should also be improved to reduce the final cost due to product separation. In addition, new efforts should be made to develop a PEMFC-like electrochemical reactor fed only with humidified CO_2, which could achieve liquid-electrolyte-free CO_2RR, at least in the cathode side, as reported in a few cases[24,25,128,129], promoting the formation of hydrocarbons and completely avoiding issues related to the low solubility of CO_2 in water.

Numerous reports have correlated CO_2RR reactivity trends to specific catalyst structure and electrolyte configurations, highlighting the role played by the catalyst morphology, including its size, shape, defect density, composition and oxidation state as well as the chemical effect of electrolytes. Various possibilities have been theoretically proposed as plausible reaction pathways and active sites for each specific product of interest, although experimental verification under operando reaction conditions is still needed. Unfortunately, many calculations still only consider the thermodynamically free energy of reactants, intermediates and products, neglecting the effect of the electrolyte and the applied field. To understand electrified solid–liquid and solid–liquid–gas interfaces in electrochemical reactions, theoretical models are needed that take into account the effect of both the potential and the electrolyte explicitly[130]. For example, a proper surface solvation model of the electrolyte–electrode interface could help determine whether alkali metal cations can be adsorbed on metal surfaces under CO_2RR conditions[62,131].

More importantly, the identification of active sites strongly relies on the precision of the characterization techniques employed, which is actually heavily restricted under the usual complex electrochemical conditions. The possible changes in oxidation state, structure and even morphology of the catalysts in air after a given CO_2RR treatment make it difficult to identify active sites from experimental results collected ex situ before and after the reaction.

Therefore, serious efforts are already being made, and more will need to be made in the years to come, to further develop operando characterization techniques compatible with a liquid environment under CO_2RR conditions, including flow cell electrolyzer configurations that could effectively address the mass transport issues in the current in situ cells[16,17]. Furthermore, there is an urgent need to improve signal intensities of some in situ and operando scattering and spectroscopy techniques due to the low coverages of key reaction intermediates. Promising methods include XAS[26,57], XPS[44,45,74], FTIR[10,116], Raman[49,55,132,133], DEMS[11,113], EC-AFM[45], EC-STM[108] and Liquid-TEM[134]. With a synergistic combination of these tools, the identification of active sites and key reaction intermediates for the distinct reaction pathways that might be preferred under different electrode and electrolyte combinations will be possible. A closer interaction between experimental and theoretical groups in this field is also highly desirable, since it could serve to validate some of the new theoretical approaches that are currently being proposed to address the complexity of real CO_2RR catalysts and electrolytes[62,130]. Furthermore, it will provide predictive guidance to the experimentalists searching for optimized material structures and compositions, and the most favourable electrolytes.

References

1. Montoya, J. H. et al. Materials for solar fuels and chemicals. *Nat. Mater.* **16**, 70–81 (2017).
2. Haas, T., Krause, R., Weber, R., Demler, M. & Schmid, G. Technical photosynthesis involving CO_2 electrolysis and fermentation. *Nat. Catal.* **1**, 32–39 (2018).
3. Nielsen, D. U., Hu, X.-M., Daasbjerg, K. & Skrydstrup, T. Chemically and electrochemically catalysed conversion of CO_2 to CO with follow-up utilization to value-added chemicals. *Nat. Catal.* **1**, 244–254 (2018).
4. Whipple, D. T. & Kenis, P. J. A. Prospects of CO_2 utilization via direct heterogeneous electrochemical reduction. *J. Phys. Chem. Lett.* **1**, 3451–3458 (2010).
5. Gao, D., Cai, F., Wang, G. & Bao, X. Nanostructured heterogeneous catalysts for electrochemical reduction of CO_2. *Curr. Opin. Green Sustain. Chem.* **3**, 39–44 (2017).
6. Kortlever, R., Shen, J., Schouten, K. J. P., Calle-Vallejo, F. & Koper, M. T. M. Catalysts and reaction pathways for the electrochemical reduction of carbon dioxide. *J. Phys. Chem. Lett.* **6**, 4073–4082 (2015).
7. Lum, Y. & Ager, J. W. Evidence for product specific sites on oxide-derived Cu catalysts for electrochemical CO_2 reduction. *Nat. Catal.* **2**, 86–93 (2019).
8. Montoya, J. H., Shi, C., Chan, K. & Nørskov, J. K. Theoretical insights into a CO dimerization mechanism in CO_2 electroreduction. *J. Phys. Chem. Lett.* **6**, 2032–2037 (2015).
9. Schouten, K. J. P., Qin, Z., Gallent, E. P. & Koper, M. T. M. Two pathways for the formation of ethylene in CO reduction on single-crystal copper electrodes. *J. Am. Chem. Soc.* **134**, 9864–9867 (2012).
10. Perez-Gallent, E., Figueiredo, M. C., Calle-Vallejo, F. & Koper, M. T. M. Spectroscopic observation of a hydrogenated CO dimer intermediate during CO reduction on Cu(100) electrodes. *Angew. Chem. Int. Ed.* **56**, 3621–3624 (2017).
    The first spectroscopic observation of a hydrogenated CO dimer Intermediate (*OCCOH) on Cu(100) during CO reduction using operando IR spectroscopy.
11. Clark, E. L. & Bell, A. T. Direct observation of the local reaction environment during the electrochemical reduction of CO_2. *J. Am. Chem. Soc.* **140**, 7012–7020 (2018).
12. Bertheussen, E. et al. Acetaldehyde as an intermediate in the electroreduction of carbon monoxide to ethanol on oxide-derived copper. *Angew. Chem. Int. Ed.* **55**, 1450–1454 (2016).
13. Arán-Ais, R. M., Gao, D. & Roldan Cuenya, B. Structure- and electrolyte-sensitivity in CO_2 electroreduction. *Acc. Chem. Res.* **51**, 2906–2917 (2018).
14. Larrazábal, G. O., Martín, A. J. & Pérez-Ramírez, J. Building blocks for high performance in electrocatalytic CO_2 reduction: materials, optimization strategies, and device engineering. *J. Phys. Chem. Lett.* **8**, 3933–3944 (2017).

15. Zhu, D. D., Liu, J. L. & Qiao, S. Z. Recent advances in inorganic heterogeneous electrocatalysts for reduction of carbon dioxide. *Adv. Mater.* **28**, 3423–3452 (2016).

16. Handoko, A. D., Wei, F., Jenndy, Yeo, B. S. & Seh, Z. W. Understanding heterogeneous electrocatalytic carbon dioxide reduction through operando techniques. *Nat. Catal.* **1**, 922–934 (2018).

17. Choi, Y. W., Mistry, H. & Roldan Cuenya, B. New insights into working nanostructured electrocatalysts through operando spectroscopy and microscopy. *Curr. Opin. Electrochem.* **1**, 95–103 (2017).

18. Weekes, D. M., Salvatore, D. A., Reyes, A., Huang, A. & Berlinguette, C. P. Electrolytic CO_2 reduction in a flow cell. *Acc. Chem. Res.* **51**, 910–918 (2018).

19. Dinh, C. T. et al. CO_2 electroreduction to ethylene via hydroxide-mediated copper catalysis at an abrupt interface. *Science* **360**, 783–787 (2018). **Ethylene was selectively produced with 70% FE at −0.55 V versus RHE in a flow cell with GDE configuration and highly alkaline electrolyte**.

20. Reske, R., Mistry, H., Behafarid, F., Roldan Cuenya, B. & Strasser, P. Particle size effects in the catalytic electroreduction of CO_2 on Cu nanoparticles. *J. Am. Chem. Soc.* **136**, 6978–6986 (2014).

21. Mistry, H. et al. Exceptional size-dependent activity enhancement in the electroreduction of CO_2 over Au nanoparticles. *J. Am. Chem. Soc.* **136**, 16473–16476 (2014).

22. Mistry, H., Reske, R., Strasser, P. & Roldan Cuenya, B. Size-dependent reactivity of gold–copper bimetallic nanoparticles during CO_2 electroreduction. *Catal. Today* **288**, 30–36 (2017).

23. Jeon, H. S. et al. Operando evolution of the structure and oxidation state of size-controlled Zn nanoparticles during CO_2 electroreduction. *J. Am. Chem. Soc.* **140**, 9383–9386 (2018).

24. Merino-Garcia, I., Albo, J. & Irabien, A. Tailoring gas-phase CO_2 electroreduction selectivity to hydrocarbons at Cu nanoparticles. *Nanotechnology* **29**, 014001 (2018).

25. Ampelli, C. et al. Electrocatalytic conversion of CO_2 to produce solar fuels in electrolyte or electrolyte-less configurations of PEC cells. *Faraday Discuss.* **183**, 125–145 (2015).

26. Roth, C. et al. Determination of O[H] and CO coverage and adsorption sites on PtRu electrodes in an operating PEM fuel cell. *J. Am. Chem. Soc.* **127**, 14607–14615 (2005).

27. Velasco-Vélez, J.-J. et al. The role of the copper oxidation state in the electrocatalytic reduction of CO_2 into valuable hydrocarbons. *ACS Sustain. Chem. Eng.* **7**, 1485–1492 (2019).

28. Saveleva, V. A. et al. Operando evidence for a universal oxygen evolution mechanism on thermal and electrochemical iridium oxides. *J. Phys. Chem. Lett.* **9**, 3154–3160 (2018).

29. Wiltshire, R. J. K. et al. A PEM fuel cell for in situ XAS studies. *Electrochim. Acta* **50**, 5208–5217 (2005).

30. Mistry, H. et al. Tuning catalytic selectivity at the mesoscale via interparticle interactions. *ACS Catal.* **6**, 1075–1080 (2016).

31. Kim, D., Kley, C. S., Li, Y. & Yang, P. Copper nanoparticle ensembles for selective electroreduction of CO_2 to C_2–C_3 products. *Proc. Natl Acad. Sci. USA* **114**, 10560–10565 (2017).

32. Wang, X., Varela, A. S., Bergmann, A., Kühl, S. & Strasser, P. Catalyst particle density controls hydrocarbon product selectivity in CO_2 electroreduction on CuO_x. *ChemSusChem* **10**, 4642–4649 (2017).

33. Hori, Y., Takahashi, I., Koga, O. & Hoshi, N. Selective formation of C_2 compounds from electrochemical reduction of CO_2 at a series of copper single crystal electrodes. *J. Phys. Chem. B* **106**, 15–17 (2002).

34. Huang, Y., Handoko, A. D., Hirunsit, P. & Yeo, B. S. Electrochemical reduction of CO_2 using copper single-crystal surfaces: effects of CO* coverage on the selective formation of ethylene. *ACS Catal.* **7**, 1749–1756 (2017).

35. Durand, W. J., Peterson, A. A., Studt, F., Abild-Pedersen, F. & Nørskov, J. K. Structure effects on the energetics of the electrochemical reduction of CO_2 by copper surfaces. *Surf. Sci.* **605**, 1354–1359 (2011).

36. Hahn, C. et al. Engineering Cu surfaces for the electrocatalytic conversion of CO_2: controlling selectivity toward oxygenates and hydrocarbons. *Proc. Natl Acad. Sci. USA* **114**, 5918–5923 (2017).

37. Peterson, A. A., Abild-Pedersen, F., Studt, F., Rossmeisl, J. & Nørskov, J. K. How copper catalyzes the electroreduction of CO_2 into hydrocarbon fuels. *Energy Environ. Sci.* **3**, 1311 (2010).

38. Calle-Vallejo, F. & Koper, M. T. M. Theoretical considerations on the electroreduction of CO to C_2 Species on Cu(100) electrodes. *Angew. Chem. Int. Ed.* **52**, 7282–7285 (2013).

39. Kim, Y. G., Javier, A., Baricuatro, J. H. & Soriaga, M. P. Regulating the product distribution of CO reduction by the atomic-level structural modification of the Cu electrode surface. *Electrocatalysis* **7**, 391–399 (2016).

40. Schouten, K. J. P., Pérez Gallent, E. & Koper, M. T. M. Structure sensitivity of the electrochemical reduction of carbon monoxide on copper single crystals. *ACS Catal.* **3**, 1292–1295 (2013).

41. Chen, C. S. et al. Stable and selective electrochemical reduction of carbon dioxide to ethylene on copper mesocrystals. *Catal. Sci. Technol.* **5**, 161–168 (2015).

42. Roberts, F. S., Kuhl, K. P. & Nilsson, A. High selectivity for ethylene from CO_2 reduction over copper nanocube electrocatalysts. *Angew. Chem. Int. Ed.* **54**, 5179–5182 (2015).

43. Loiudice, A. et al. Tailoring copper nanocrystals towards C_2 products in electrochemical CO_2 reduction. *Angew. Chem. Int. Ed.* **55**, 5789–5792 (2016).

44. Gao, D. et al. Plasma-activated copper nanocube catalysts for efficient carbon dioxide electroreduction to hydrocarbons and alcohols. *ACS Nano* **11**, 4825–4831 (2017).

45. Grosse, P. et al. Dynamic changes in the structure, chemical state and catalytic selectivity of Cu nanocubes during CO_2 electroreduction: size and support effects. *Angew. Chem. Int. Ed.* 6192–6197 (2018). **Dynamic changes of morphological and chemical states of Cu nanocubes during CO_2 RR were monitored using operando EC-AFM and EXAFS and correlated to the activity and selectivity**.

46. Dutta, A., Rahaman, M., Luedi, N. C., Mohos, M. & Broekmann, P. Morphology matters: Tuning the product distribution of CO_2 electroreduction on oxide-derived Cu foam catalysts. *ACS Catal.* **6**, 3804–3814 (2016).

47. Dutta, A., Rahaman, M., Mohos, M., Zanetti, A. & Broekmann, P. Electrochemical CO_2 conversion using skeleton (sponge) type of Cu catalysts. *ACS Catal.* **7**, 5431–5437 (2017).

48. Reller, C. et al. Selective electroreduction of CO_2 toward ethylene on nano dendritic copper catalysts at high current density. *Adv. Energy Mater.* **7**, 1602114 (2017).

49. Klingan, K. et al. Reactivity determinants in electrodeposited Cu foams for electrochemical CO_2 reduction. *ChemSusChem* **11**, 3449–3459 (2018).

50. Jeon, H. S., Kunze, S., Scholten, F. & Roldan Cuenya, B. Prism-shaped Cu nanocatalysts for electrochemical CO_2 reduction to ethylene. *ACS Catal.* **8**, 531–535 (2018).

51. Mariano, R. G., McKelvey, K., White, H. S. & Kanan, M. W. Selective increase in CO_2 electroreduction activity at grain-boundary surface terminations. *Science* **358**, 1187–1192 (2017).

52. Tang, W. et al. The importance of surface morphology in controlling the selectivity of polycrystalline copper for CO_2 electroreduction. *Phys. Chem. Chem. Phys.* **14**, 76–81 (2012).

53. Gupta, N., Gattrell, M. & MacDougall, B. Calculation for the cathode surface concentrations in the electrochemical reduction of CO_2 in $KHCO_3$ solutions. *J. Appl. Electrochem.* **36**, 161–172 (2006).

54. Pander, J. E. et al. Understanding the heterogeneous electrocatalytic reduction of CO_2 on oxide-derived catalysts. *ChemElectroChem* **5**, 219–237 (2018).

55. Mandal, L. et al. Investigating the role of copper oxide in electrochemical CO_2 reduction in real time. *ACS Appl. Mater. Interfaces* **10**, 8574–8584 (2018).

56. Lum, Y. & Ager, J. W. Stability of residual oxides in oxide-derived copper catalysts for electrochemical CO_2 reduction investigated with ^{18}O labeling. *Angew. Chem. Int. Ed.* **57**, 551–554 (2018).

57. Mistry, H. et al. Highly selective plasma-activated copper catalysts for CO_2 reduction to ethylene. *Nat. Commun.* **7**, 12123 (2016).

58. Favaro, M. et al. Subsurface oxide plays a critical role in CO_2 activation by Cu(111) surfaces to form chemisorbed CO_2, the first step in reduction of CO_2. *Proc. Natl Acad. Sci. USA* **114**, 6706–6711 (2017).

59. Xiao, H., Goddard, W., Cheng, T. & Liu, Y. Cu metal embedded in oxidized matrix catalyst to promote CO_2 activation and CO dimerization for electrochemical reduction of CO_2. *Proc. Natl Acad. Sci. USA* **114**, 6685–6688 (2017). **The interface between Cu^+ and Cu^0 species significantly improves the kinetics and thermodynamics of both CO_2 activation, and CO dimerization**.

60. Zhou, Y. et al. Dopant-induced electron localization drives CO_2 reduction to C_2 hydrocarbons. *Nat. Chem.* **10**, 947–980 (2018).

61. Gao, D., Scholten, F. & Roldan Cuenya, B. Improved CO_2 electroreduction performance on plasma-activated Cu catalysts via electrolyte design: Halide effect. *ACS Catal.* **7**, 5112–5120 (2017).

62. Gao, D. et al. Activity and selectivity control in CO_2 electroreduction to multicarbon products over CuO_x catalysts via electrolyte design. *ACS Catal.* **8**, 10012–10020 (2018). **By combining experiment and DFT calculations, a synergistic effect of the electrolyte (larger cations, halides) and the presence of subsurface oxygen species was found to stabilize Cu^+ species during CO_2RR and improve the C_{2+} production and stability of CuO_x catalysts**.

63. Wang, L. et al. Electrochemical carbon monoxide reduction on polycrystalline copper: Effects of potential, pressure, and pH on selectivity toward multicarbon and oxygenated products. *ACS Catal.* **8**, 7445–7454 (2018).

64. Clark, E. L. et al. Standards and protocols for data acquisition and reporting for studies of the electrochemical reduction of carbon dioxide. *ACS Catal.* **8**, 6560–6570 (2018).

65. Schlögl, R. Heterogeneous catalysis. *Angew. Chem. Int. Ed.* **54**, 3465–3520 (2015).

66. Garza, A. J., Bell, A. T. & Head-Gordon, M. Is subsurface oxygen necessary for the electrochemical reduction of CO_2 on copper? *J. Phys. Chem. Lett.* **9**, 601–606 (2018).

67. Yin, Z. et al. Highly selective palladium-copper bimetallic electrocatalysts for the electrochemical reduction of CO_2 to CO. *Nano Energy* **27**, 35–43 (2016).

68. Ma, S. et al. Electroreduction of CO_2 to hydrocarbons using bimetallic Cu–Pd catalysts with different mixing patterns. *J. Am. Chem. Soc.* **139**, 47–50 (2017). **Phase-separated Cu–Pd bimetallic NPs achieved higher selectivity (>60%) for C_2 chemicals than ordered and disordered ones. Geometric effects rather than electronic effects seem to be key in determining the selectivity of bimetallic Cu–Pd catalysts.**

69. Chen, D. et al. Tailoring the selectivity of bimetallic copper-palladium nanoalloys for electrocatalytic reduction of CO_2 to CO. *ACS Appl. Energy Mater.* **1**, 883–890 (2018).

70. Li, M. et al. Mesoporous palladium-copper bimetallic electrodes for selective electrocatalytic reduction of aqueous CO_2 to CO. *J. Mater. Chem. A* **4**, 4776–4782 (2016).

71. Mavrikakis, M., Hammer, B. & Nørskov, J. K. Effect of strain on the reactivity of metal surfaces. *Phys. Rev. Lett.* **81**, 2819–2822 (1998).

72. Bligaard, T. & Nørskov, J. K. Ligand effects in heterogeneous catalysis and electrochemistry. *Electrochim. Acta* **52**, 5512–5516 (2007).

73. Reske, R. et al. Controlling catalytic selectivities during CO_2 electroreduction on thin Cu metal overlayers. *J. Phys. Chem. Lett.* **4**, 2410–2413 (2013).

74. Bernal, M. et al. CO_2 electroreduction on copper-cobalt nanoparticles: Size and composition effect. *Nano Energy* **53**, 27–36 (2018).

75. Kim, D., Resasco, J., Yu, Y., Asiri, A. M. & Yang, P. Synergistic geometric and electronic effects for electrochemical reduction of carbon dioxide using gold-copper bimetallic nanoparticles. *Nat. Commun.* **5**, 4948 (2014).

76. Kim, D. et al. Electrochemical activation of CO_2 through atomic ordering transformations of AuCu nanoparticles. *J. Am. Chem. Soc.* **139**, 8329–8336 (2017).

77. Ren, D., Ang, B. S. H. & Yeo, B. S. Tuning the selectivity of carbon dioxide electroreduction toward ethanol on oxide-derived Cu_xZn catalysts. *ACS Catal.* **6**, 8239–8247 (2016). The CO spillover effect was observed and applied to facilitate selective **CO_2RR to ethanol on oxide-derived Cu_x Zn catalysts.**

78. Lee, S., Park, G. & Lee, J. Importance of Ag–Cu biphasic boundaries for selective electrochemical reduction of CO_2 to ethanol. *ACS Catal.* **7**, 8594–8604 (2017).

79. Clark, E. L., Hahn, C., Jaramillo, T. F. & Bell, A. T. Electrochemical CO_2 reduction over compressively strained CuAg surface alloys with enhanced multi-carbon oxygenate selectivity. *J. Am. Chem. Soc.* **139**, 15848–15857 (2017).

80. He, J., Johnson, N. J. J., Huang, A. & Berlinguette, C. P. Electrocatalytic alloys for CO_2 reduction. *ChemSusChem* **11**, 48–57 (2018).

81. Lum, Y. & Ager, J. W. Sequential catalysis controls selectivity in electrochemical CO_2 reduction on Cu. *Energy Environ. Sci.* **11**, 2935–2944 (2018).

82. Morales-Guio, C. G. et al. Improved CO_2 reduction activity towards C_{2+} alcohols on a tandem gold on copper electrocatalyst. *Nat. Catal.* **1**, 764–771 (2018).

83. Jovanov, Z. P. et al. Opportunities and challenges in the electrocatalysis of CO_2 and CO reduction using bifunctional surfaces: a theoretical and experimental study of Au–Cd alloys. *J. Catal.* **343**, 215–231 (2016).

84. Kortlever, R. et al. Palladium–gold catalyst for the electrochemical reduction of CO_2 to C_1–C_5 hydrocarbons. *Chem. Commun.* **52**, 10229–10232 (2016).

85. Torelli, D. A. et al. Nickel–gallium-catalyzed electrochemical reduction of CO_2 to highly reduced products at low overpotentials. *ACS Catal.* **6**, 2100–2104 (2016).

86. Paris, A. R. & Bocarsly, A. B. Ni–Al films on glassy carbon electrodes generate an array of oxygenated organics from CO_2. *ACS Catal.* **7**, 6815–6820 (2017).

87. Verdaguer-Casadevall, A. et al. Probing the active surface sites for CO reduction on oxide-derived copper electrocatalysts. *J. Am. Chem. Soc.* **137**, 9808–9811 (2015).

88. Dutta, A., Morstein, C. E., Rahaman, M., Cedeño López, A. & Broekmann, P. Beyond copper in CO_2 electrolysis: effective hydrocarbon production on silver nano-foam catalysts. *ACS Catal.* **8**, 8357–8368 (2018). **By creating high density of defects and lower-coordinated sites, one could transform a CO-producing catalyst (with weak CO binding) into a hydrocarbon- and alcohol-producing catalyst.**

89. Mistry, H. et al. Enhanced CO_2 electroreduction to CO over defect-rich plasma-activated silver catalysts. *Angew. Chem. Int. Ed.* **56**, 11394–11398 (2017).

90. Michalsky, R., Zhang, Y. J., Medford, A. J. & Peterson, A. A. Departures from the adsorption energy scaling relations for metal carbide catalysts. *J. Phys. Chem. C* **118**, 13026–13034 (2014).

91. Kim, S. K., Zhang, Y. J., Bergstrom, H., Michalsky, R. & Peterson, A. Understanding the low-overpotential production of CH_4 from CO_2 on Mo_2C catalysts. *ACS Catal.* **6**, 2003–2013 (2016).

92. Chan, K., Tsai, C., Hansen, H. A. & Nørskov, J. K. Molybdenum sulfides and selenides as possible electrocatalysts for CO_2 reduction. *ChemCatChem* **6**, 1899–1905 (2014).

93. Francis, S. A. et al. Reduction of aqueous CO_2 to 1-propanol at MoS_2 electrodes. *Chem. Mater.* **30**, 4902–4908 (2018).

94. Calvinho, K. U. D. et al. Selective CO_2 reduction to C_3 and C_4 oxyhydrocarbons on nickel phosphides at overpotentials as low as 10 mV. *Energy Environ. Sci.* **11**, 2550–2559 (2018).

95. Back, S. & Jung, Y. TiC- and TiN-supported single-atom catalysts for dramatic improvements in CO_2 electrochemical reduction to CH_4. *ACS Energy Lett.* **2**, 969–975 (2017).

96. Cheng, M. J., Clark, E. L., Pham, H. H., Bell, A. T. & Head-Gordon, M. Quantum mechanical screening of single-atom bimetallic alloys for the selective reduction of CO_2 to C_1 hydrocarbons. *ACS Catal.* **6**, 7769–7777 (2016).

97. Back, S., Lim, J., Kim, N. Y., Kim, Y. H. & Jung, Y. Single-atom catalysts for CO_2 electroreduction with significant activity and selectivity improvements. *Chem. Sci.* **8**, 1090–1096 (2017).

98. Ju, W. et al. Understanding activity and selectivity of metal-nitrogen-doped carbon catalysts for electrochemical reduction of CO_2. *Nat. Commun.* **8**, 944 (2017).

99. Bagger, A., Ju, W., Varela, A. S., Strasser, P. & Rossmeisl, J. Single site porphyrine-like structures advantages over metals for selective electrochemical CO_2 reduction. *Catal. Today* **288**, 74–78 (2017).

100. Genovese, C. et al. Operando spectroscopy study of the carbon dioxide electro-reduction by iron species on nitrogen-doped carbon. *Nat. Commun.* **9**, 935 (2018).

101. Wu, J. et al. A metal-free electrocatalyst for carbon dioxide reduction to multi-carbon hydrocarbons and oxygenates. *Nat. Commun.* **7**, 13869 (2016). **The N-doped graphene quantum dots showed a high total CO_2RR FE of up to 90%, with the C_2 and C_3 product distribution and production rate comparable to those obtained with copper nanoparticle-based electrocatalysts.**

102. Liu, Y., Chen, S., Quan, X. & Yu, H. Efficient electrochemical reduction of carbon dioxide to acetate on nitrogen-doped nanodiamond. *J. Am. Chem. Soc.* **137**, 11631–11636 (2015).

103. Liu, Y. et al. Selective electrochemical reduction of carbon dioxide to ethanol on a boron- and nitrogen-co-doped nanodiamond. *Angew. Chem. Int. Ed.* **56**, 15607–15611 (2017).

104. Nakata, K., Ozaki, T., Terashima, C., Fujishima, A. & Einaga, Y. High-yield electrochemical production of formaldehyde from CO_2 and seawater. *Angew. Chem. Int. Ed.* **53**, 871–874 (2014).

105. Song, Y. et al. Metal-free nitrogen-doped mesoporous carbon for electroreduction of CO_2 to ethanol. *Angew. Chem. Int. Ed.* **56**, 10840–10844 (2017).

106. Huang, J. et al. Potential-induced nanoclustering of metallic catalysts during electrochemical CO_2 reduction. *Nat. Commun.* **9**, 3117 (2018).

107. Kim, Y.-G., Baricuatro, J. H. & Soriaga, M. P. Surface reconstruction of polycrystalline Cu electrodes in aqueous $KHCO_3$ electrolyte at potentials in the early stages of CO_2 reduction. *Electrocatalysis* **9**, 526–530 (2018).

108. Kim, Y. G., Baricuatro, J. H., Javier, A., Gregoire, J. M. & Soriaga, M. P. The evolution of the polycrystalline copper surface, first to Cu(111) and then to Cu(100), at a fixed CO_2RR potential: a study by operando EC-STM. *Langmuir* **30**, 15053–15056 (2014). **An operando EC-STM study showed the surface reconstruction from a polycrystalline Cu electrode first to Cu(111), and then to Cu(100) under CO_2 RR conditions.**

109. Jiang, K. et al. Metal ion cycling of Cu foil for selective C–C coupling in electrochemical CO_2 reduction. *Nat. Catal.* **1**, 111–119 (2018).

110. Lee, S. Y. et al. Mixed copper states in anodized Cu electrocatalyst for stable and selective ethylene production from CO_2 reduction. *J. Am. Chem. Soc.* **140**, 8681–8689 (2018).

111. Singh, M. R., Kwon, Y., Lum, Y., Ager, J. W. & Bell, A. T. Hydrolysis of electrolyte cations enhances the electrochemical reduction of CO_2 over Ag and Cu. *J. Am. Chem. Soc.* **138**, 13006–13012 (2016).

112. Resasco, J. et al. Promoter effects of alkali metal cations on the electrochemical reduction of carbon dioxide. *J. Am. Chem. Soc.* **139**, 11277–11287 (2017).

113. Pérez-Gallent, E., Marcandalli, G., Figueiredo, M. C., Calle-Vallejo, F. & Koper, M. T. M. Structure- and potential-dependent cation effects on CO reduction at copper single-crystal electrodes. *J. Am. Chem. Soc.* **139**, 16412–16419 (2017).

114. Ayemoba, O. & Cuesta, A. Spectroscopic evidence of size-dependent buffering of interfacial pH by cation hydrolysis during CO_2 electroreduction. *ACS Appl. Mater. Interfaces* **9**, 27377–27382 (2017).

115. Schizodimou, A. & Kyriacou, G. Acceleration of the reduction of carbon dioxide in the presence of multivalent cations. *Electrochim. Acta* **78**, 171–176 (2012).

116. Dunwell, M. et al. The central role of bicarbonate in the electrochemical reduction of CO_2 on gold. *J. Am. Chem. Soc.* **139**, 3774–3783 (2017).

117. Zhu, S., Jiang, B., Cai, W. & Shao, M. Direct observation on reaction intermediates and the role of bicarbonate anions in CO_2 electrochemical reduction reaction on Cu surfaces. *J. Am. Chem. Soc.* **139**, 15664–15667 (2017).

118. Wuttig, A., Yoon, Y., Ryu, J. & Surendranath, Y. Bicarbonate is not a general acid in Au-catalyzed CO_2 electroreduction. *J. Am. Chem. Soc.* **139**, 17109–17113 (2017).

119. Huang, Y., Ong, C. W. & Yeo, B. S. Effects of electrolyte anions on the reduction of carbon dioxide to ethylene and ethanol on copper (100) and (111) surfaces. *ChemSusChem* **11**, 3299–3306 (2018).

120. McCrum, I. T., Akhade, S. A. & Janik, M. J. Electrochemical specific adsorption of halides on Cu 111,100, and 211: A density functional theory study. *Electrochim. Acta* **173**, 302–309 (2015).

121. Varela, A. S., Ju, W., Reier, T. & Strasser, P. Tuning the catalytic activity and selectivity of Cu for CO_2 electroreduction in the presence of halides. *ACS Catal.* **6**, 2136–2144 (2016).

122. Schouten, K. J. P., Pérez Gallent, E. & Koper, M. T. M. The influence of pH on the reduction of CO and CO_2 to hydrocarbons on copper electrodes. *J. Electroanal. Chem.* **716**, 53–57 (2014).

123. Jouny, M., Luc, W. & Jiao, F. High-rate electroreduction of carbon monoxide to multi-carbon products. *Nat. Catal.* **1**, 748–755 (2018).

124. Todoroki, M., Hara, K., Kudo, A. & Sakata, T. Electrochemical reduction of high pressure CO_2 at Pb, Hg and In electrodes in an aqueous $KHCO_3$ solution. *J. Electroanal. Chem.* **394**, 199–203 (1995).

125. Melchaeva, O. et al. Electrochemical reduction of protic supercritical CO_2 on copper electrodes. *ChemSusChem* **10**, 3660–3670 (2017).

126. Rosen, B. A. et al. Ionic liquid-mediated selective conversion of CO_2 to CO at low overpotentials. *Science* **334**, 643–644 (2011).

127. Sun, X. et al. Design of a Cu(i)/C-doped boron nitride electrocatalyst for efficient conversion of CO_2 into acetic acid. *Green Chem.* **19**, 2086–2091 (2017).

128. Pătru, A., Binninger, T., Pribyl, B. & Schmidt, T. J. Design principles of bipolar electrochemical co-electrolysis cells for efficient reduction of carbon dioxide from gas phase at low temperature. *J. Electrochem. Soc.* **166**, F34–F43 (2019).

129. Gao, D. et al. Gas-phase electrocatalytic reduction of carbon dioxide using electrolytic cell based on phosphoric acid-doped polybenzimidazole membrane. *J. Energy Chem.* **23**, 694–700 (2014).

130. Goodpaster, J. D., Bell, A. T. & Head-Gordon, M. Identification of possible pathways for C–C bond formation during electrochemical reduction of CO_2: new theoretical insights from an improved electrochemical model. *J. Phys. Chem. Lett.* **7**, 1471–1477 (2016).

131. Mills, J. N., McCrum, I. T. & Janik, M. J. Alkali cation specific adsorption onto fcc(111) transition metal electrodes. *Phys. Chem. Chem. Phys.* **16**, 13699–13707 (2014).

132. Deng, Y. & Yeo, B. S. Characterization of electrocatalytic water splitting and CO_2 reduction reactions using in situ/operando Raman spectroscopy. *ACS Catal.* **7**, 7873–7889 (2017).

133. Dutta, A., Kuzume, A., Rahaman, M., Vesztergom, S. & Broekmann, P. Monitoring the chemical state of catalysts for CO_2 electroreduction: an in operando study. *ACS Catal.* **5**, 7498–7502 (2015).

134. Zhu, C. et al. In-situ liquid cell transmission electron microscopy investigation on oriented attachment of gold nanoparticles. *Nat. Commun.* **9**, 421 (2018).

Acknowledgements

Competing interests

The authors declare no competing interests.

Additional information

Reprints and permissions information is available at www.nature.com/reprints.

Correspondence should be addressed to B.R.

Publisher's note: Springer Nature remains neutral with regard to jurisdictional claims in published maps and institutional affiliations.